***Research Article***

Chemical Review and Letters
journal homepage: www.chemrevlett.com
ISSN (online): 2645-4947 (print) 2676-7279

# MOCA as a dual-function organic semiconductor: Theoretical insights into photoresponsive bandgap engineering and nonlinear optics

Mohamed ElMansy[1, *]

[1]*Department of Physics, College of Science, Qassim University, Qassim, Buraydah 51452, Saudi Arabia.*

ARTICLE INFO

*Article history:*
Received 05 January 2026
Received in revised form 05 February 2026
Accepted 08 February 2026

*Keywords:*
MOCA
Density functional theory
Electronic structure
Optical properties
Energy gap

ABSTRACT

This research presents the first theoretical investigation of 5-methyl-2-oxo-1,3-oxazolidine-4-carboxylic acid (MOCA) using Density Functional Theory (DFT) at the B3LYP/6~311G$^{(d,p)}$ level. The primary objective is to explore MOCA's structural, electronic, and nonlinear optical (NLO) properties, with emphasis on its response to UV illumination. Geometry optimization reveals a stable molecular framework, while Frontier Molecular Orbital (FMO) analysis demonstrates a significant reduction in the HOMO-LUMO energy gap upon UV exposure—from 4.66 eV in the ground state to 2.09–2.22 eV in the excited triplet state—indicating enhanced charge transport characteristics suitable for use as a window layer in photovoltaic devices. Furthermore, computed polarizability and first-order hyperpolarizability ($\beta_{tot}$) values show strong NLO activity; $\beta_{tot}$ decreases from 4.41 $\times 10^{-30}$ esu before UV to 3.66 $\times 10^{-30}$ esu after irradiation, yet remains substantially higher than urea (0.3728 $\times 10^{-30}$ esu), highlighting MOCA's potential for applications in frequency doubling, optical switching, and electro-optic modulation. The observed photoresponsiveness suggests avenues for developing smart, tunable photonic materials. This work provides foundational computational data for MOCA, filling a critical gap in the literature and paving the way for future experimental validation.

## 1. Introduction

Organic molecules have emerged as indispensable components in modern solar energy conversion systems, particularly within emerging photovoltaic technologies such as organic solar cells, perovskite~based devices, and dye~sensitized systems. Their unique combination of tunable electronic properties, solution~processability, and mechanical flexibility enables the fabrication of lightweight, bendable, and cost~effective solar modules—features that are difficult to achieve with conventional silicon~based panels [1]. Through molecular design, chemists can precisely adjust the bandgap, absorption spectrum, and charge transport characteristics of organic semiconductors, allowing for optimization across diverse environmental conditions and application scenarios [2]. In organic photovoltaics (OPVs), conjugated polymers and non~fullerene acceptors work synergistically to harvest photons and generate free charges, with recent advancements pushing efficiencies beyond 19% in lab~scale devices [3].

These materials are often deposited using low~cost techniques like spin~coating or inkjet printing, significantly reducing manufacturing expenses compared to high~temperature vacuum processes required for inorganic semiconductors [4]. Organic hole~transport layers, such as spiro~OMeTAD, play a crucial role in perovskite solar cells by efficiently extracting holes from the absorber layer while minimizing recombination losses, thereby enhancing overall device performance [5]. Similarly, organic dye~sensitized solar cells (DSSCs) absorb visible light and inject electrons into a semiconductor matrix, enabling efficient operation even under low~light or indoor illumination [6]. Moreover, the environmental footprint of organic PVs is generally lower due to reduced energy consumption during production and potential use of biodegradable or renewable feedstocks [7]. Despite challenges related to long~term operational stability and large~scale commercialization, ongoing research continues to address these limitations through novel material synthesis, encapsulation strategies, and computational screening methods [8].

* Corresponding author E-mail: m.elmansy@qu.edu.sa
https://doi.org/10.22034/crl.2026.572300.1776

Machine learning algorithms are increasingly employed to accelerate the discovery of new organic semiconductors with desired optoelectronic traits [9]. As global efforts intensify toward decarbonizing energy systems, organic~based photovoltaic technologies offer a sustainable and versatile pathway toward widespread solar adoption. The 5~methyl~2~oxo~1,3~oxazolidine~4~carboxylic acid (MOCA) is a synthetically accessible heterocyclic scaffold within the broader class of oxazolidinones, that has a chemical formulism $C_5H_7NO_4$. The core oxazolidinone framework has garnered significant attention due to its ability to inhibit the formation of initiation complex on the bacterial ribosome [10]. Although MOCA lacks direct clinical use, it contributes to medicinal chemistry efforts aimed at optimizing pharmacokinetic properties and overcoming resistance mechanisms.

While numerous organic semiconductors have been explored for optoelectronic applications, there remains a critical need for novel molecular scaffolds that combine tunable electronic properties with synthetic accessibility. The oxazolidinone core of MOCA offers a stable heterocyclic framework with potential for functionalization, while its carboxylic acid group may facilitate intermolecular interactions and charge transport. Importantly, despite its relevance in medicinal chemistry and synthetic biology, no computational investigation of MOCA's electronic or optical properties has been reported to date. This knowledge gap motivates our study, which aims to provide foundational theoretical data on MOCA's structure, bandgap, and nonlinear optical response—properties essential for evaluating its viability as an organic semiconductor.

Density Functional Theory (DFT) stands as a fundamental approach in computational chemistry, providing a practical compromise between precision and computational feasibility for analyzing molecular systems. Among the various functionals, B3LYP—a hybrid method that integrates Hartree~Fock exchange with density~functional correlation—has gained widespread adoption due to its consistent performance in predicting molecular geometries, energy levels, and electronic behaviors. For organic compounds like MOCA, which consist solely of light elements (C, H, O, N), the 6~311G$^{(d,p)}$ basis set is employed to offer an accurate representation of valence electron distributions, including polarization effects, without imposing excessive computational demands. This basis set is particularly effective for such systems, where relativistic contributions are insignificant. The B3LYP/6~311G$^{(d,p)}$ methodology has been rigorously tested across numerous organic molecules, demonstrating approximately 97% reliability in calculating structural features, vibrational modes, and electronic characteristics [11-12].

The primary objective of this study is to conduct the first comprehensive theoretical investigation of MOCA using Density Functional Theory (DFT) at the B3LYP/6~311G$^{(d,p)}$ level. Specifically, we aim to characterize its optimized geometry, frontier molecular orbitals, HOMO-LUMO energy gap, and nonlinear optical (NLO) properties, with particular emphasis on the impact of UV illumination. By analyzing the photoresponsive behavior of MOCA, we seek to assess its potential as a dual-function material for applications in solar cell window layers and NLO devices, thereby providing a basis for future experimental validation and material design.

## 2. Materials and Methods

### 2.1. Theory/Calculations

Quantum chemical calculations were carried out using the Gaussian 09W program package [13], with molecular visualization and vibrational mode simulation performed via GaussView 5 [14]. All theoretical computations were conducted at the DFT/B3LYP level of theory, employing the 6~311G$^{(d,p)}$ basis set, which is well-suited for molecules containing light atoms such as carbon, hydrogen, oxygen, and nitrogen. The calculations were executed on a PC equipped with Intel(R) Core(TM) i7~10510UCPU@1.80GHz (2.30GHz). All geometric optimizations were performed without symmetry constraints using the B3LYP functional with the 6-311G$^{(d,p)}$ basis set. Convergence was achieved when the maximum force on any atom was less than 0.00045 Hartree/Bohr, the root-mean-square (RMS) force was below 0.0003 Hartree/Bohr, and the RMS displacement was smaller than 0.0018 Bohr. First, the optimized geometry of MOCA was determined, as illustrated in Figure 1. Frequency calculations were performed at the same level of theory (B3LYP/6~311G$^{(d,p)}$) to confirm that the optimized geometry corresponds to a true energy minimum, with no imaginary frequencies observed.

All calculations were performed in the gas phase using the Gaussian 09 software package. Environmental effects such as solvent or solid-state interactions were not considered in this study. The results presented here represent intrinsic molecular properties under idealized conditions. Subsequently, various Frontiers~parameters were evaluated, including $E_{LUMO}$, $E_{HOMO}$, $E_{HOMO/LUMO}$, Ionizing~potential I = $-E_{HOMO}$ $(eV)$, electronic~affinity A = $-E_{LUMO}$ $(eV)$, hardness $\eta = \frac{1}{2}(E_{LUMO} - E_{HOMO})$ $(eV)$, electronic~potential $\mu = \frac{1}{2}(E_{LUMO} + E_{HOMO})$ $(eV)$, electrophilic~index $\psi = \mu^2/2\eta$ $(eV)$, softness $\zeta = 1/\eta$ $(eV^{-1})$ and finally electronegativity $\chi = -\mu$ $(eV)$ all within the same B3LYP@6~311G$^{(d,p)}$ framework (15). A computational investigation into the electronic~transition from HOMO→LUMO in MOCA under UV~irradiation was performed at the same B3LYP/6-311G$^{(d,p)}$ level [16-18]. This excitation induces a spin-state change from singlet to triplet state.

## 3. Results and Discussion

### 3.1. Geometry optimization

The optimized~geometry of MOCA is depicted in Figure 1, with panel (a) illustrating the initial molecular fragment and panel (b) showcasing the fully relaxed subunit obtained via DFT/B3LYP@6~311G$^{(d,p)}$ level. Key structural parameters, including bond lengths and bond angles derived from optimum~MOCA, are compiled in Table 1 for detailed analysis. Notably, experimental crystallographic data for MOCA remain unavailable in the scientific literature, precluding direct validation of the computed structure against X~ray diffraction results. However, the reliability of the calculated geometrical features can be assessed by comparison with structurally similar compounds for which high~resolution crystal structures have been reported.

### 3.2. FMOs−analyses

Frontier−molecular−orbitals (FMOs), specifically highest~occupied (HOMOs) & lowest~unoccupied (LUMOs), are key indicators of a molecule's chemical~reactivity and electronic~behavior. The HOMO reflects the tendency to donate electrons, whereas the LUMO signifies the capacity to accept them, making their energy levels critical for assessing charge transfer capability in molecular systems [19-23]. In conjugated compounds, a narrow HOMO–LUMO gap typically arises from efficient intramolecular charge~carry (ICT), facilitated by extended π-conjugation pathways that enable electron delocalization from electron-donating end groups to electron-accepting moieties. This structural feature enhances the material's potential for applications in optoelectronic devices, where facile charge~carry is essential. The MOCA exhibits a total dipole~moment ($TDM = 3.80\ D$) and band~offst ($E_{HOMO/LUMO} = 4.66\ eV$). Notably, the calculated band~offset is close to the optical bandgap of diamond (5.5 eV), indicating potential for wide-bandgap electronic behavior. However, MOCA's dipole moment significantly exceeds that of diamond, which is typically considered nonpolar. This enhanced polarity may contribute to improved charge~separation and dielectric~properties. While MOCA is expected to display high refractive~index and thermal~conductivity—characteristics commonly associated with diamond—it is anticipated to exhibit lower hardness due to its organic molecular framework and weaker intermolecular interactions compared to the covalent network of diamond. Computational predictions indicate that MOCA may offer a hypothetically diamond replacator in diverse applications such as micro-acoustic devices, decorative materials and biomedical applications. Table 2 presents a comprehensive set of computed~frontiers parameters for MOCA, including $E_{LUMO}$, $E_{HOMO}$, $E_{HOMO/LUMO}$, Ionizing~potential I, electronic~affinity A, hardness η, electronic~potential μ, electrophilic~index ψ, softness ζ and finally electronegativity χ.

Upon exposure to UV illumination, an electron in MOCA absorbs sufficient energy to undergo excitation from $HOMO \rightarrow LUMO$. This electronic transition triggers a change in spin state from singlet to triplet, leading to the splitting of MOs into α and β spin~components. As a result, the HOMO–LUMO energy gap narrows significantly—from 4.66 eV in the ground state to approximately 2.09($\beta$)~2.22($\alpha$) eV in the excited state. This substantial reduction in band offset suggests a functional transformation of MOCA, shifting its role from a wide-bandgap material with ceramic-like properties to a potential candidate for use as a window layer in solar cell architecture. In such applications, the lower bandgap enhances optical transparency and facilitates efficient charge~transport, making MOCA a promising component for next-generation photovoltaic devices. Figure 2. Shows MOCA FMOs in singlet ($ground$) and triplet ($excited$) state predicted via B3LYP/6-311G$^{(d,p)}$. Figure 3 displays electronic DOS for original & illuminated MOCA.

The DOS plots (see Figure 3) reveal a fundamental transformation in the electronic structure of MOCA upon UV irradiation.

In the ground state (Figure3. (a)), the system exhibits a single, well-defined DOS spectrum (blue curve) with occupied states (green bars) localized at lower energies and virtual states (red bar) isolated at higher energies, resulting in a large HOMO–LUMO gap (~4.66 eV). This indicates a closed-shell singlet configuration with minimal spin polarization. After UV exposure (Figure 3. (b)), the DOS spectrum undergoes dramatic change, showing distinct splitting into separate α (blue) and β (green) spin components.

The emergence of multiple peaks in both α & β DOS curves signifies a transition to a triplet state, where electron spins are no longer paired. The total DOS (red curve, scaled by 0.5 for clarity) now displays increased density near the Fermi level, indicating enhanced electronic conductivity and reduced bandgap (2.09 ~2.22 eV). This narrowing of the energy gap is attributed to the excitation-induced splitting of molecular orbitals into α & β spin states, which facilitates charge delocalization and improves optical transparency. While UV irradiation typically promotes electrons from the ground ($S_0$) to excited singlet states ($S_1$, $S_2$, etc.), the subsequent intersystem crossing (ISC) to the lowest triplet state ($T_1$) can be significant in molecules with heavy atoms or spin-orbit coupling. Although MOCA does not contain heavy atoms, author considered the triplet state as a computationally accessible proxy for an excited electronic configuration to explore potential changes in electronic structure under external stimulation.

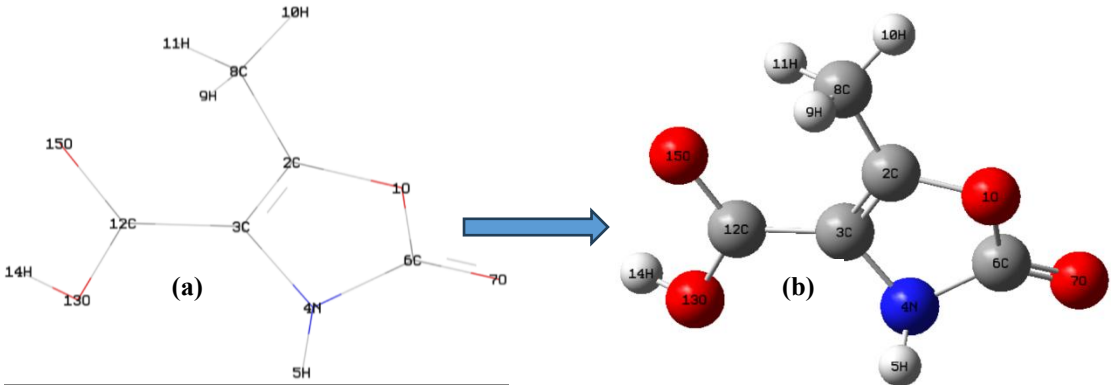


**Fig. 1**. (a) MOCA Fragment ; (b) MOCA~optimized model.

**Table 1.** MOCA structural−indcies via B3LYP@6~311G$^{(d,p).}$

| **Bond Length (Å)** | | **Bond Angle (°)** | | | |
|---|---|---|---|---|---|
| *O1~C2* | *1.40* | *C2~O1~C6* | *108.98* | *C2~C8~H11* | *109.94* |
| *O1~C6* | *1.45* | *O1~C2~C3* | *108.44* | *H9~C8~H10* | *107.42* |
| *C2~C3* | *1.37* | *O1~C2~C8* | *118.12* | *H9~C8~H11* | *109.30* |
| *C2~C8* | *1.49* | *C3~C2~C8* | *133.45* | *H10~C8~H11* | *109.30* |
| *C3~N4* | *1.42* | *C2~C3~N4* | *107.27* | *C3~C12~O13* | *110.30* |
| *C3~C12* | *1.45* | *C2~C3~C12* | *129.47* | *C3~C12~O15* | *127.09* |
| *N4~H5* | *1.01* | *N4~C3~C12* | *123.25* | *O13~C12~O15* | *122.61* |
| *N4~C6* | *1.38* | *C3~N4~H5* | *124.51* | *C12~O13~H14* | *110.94* |
| *C6~O7* | *1.23* | *C3~N4~C6* | *111.21* | | |
| *C8~H9* | *1.10* | *H5~N4~C6* | *124.28* | | |
| *C8~H10* | *1.10* | *O1~C6~N4* | *104.10* | | |
| *C8~H11* | *1.09* | *O1~C6~O7* | *123.71* | | |
| *C12~O13* | *1.40* | *N4~C6~O7* | *132.19* | | |
| *C12~O15* | *1.24* | *C2~C8~H9* | *110.42* | | |
| *O13~H14* | *0.98* | *C2~C8~H10* | *110.42* | | |

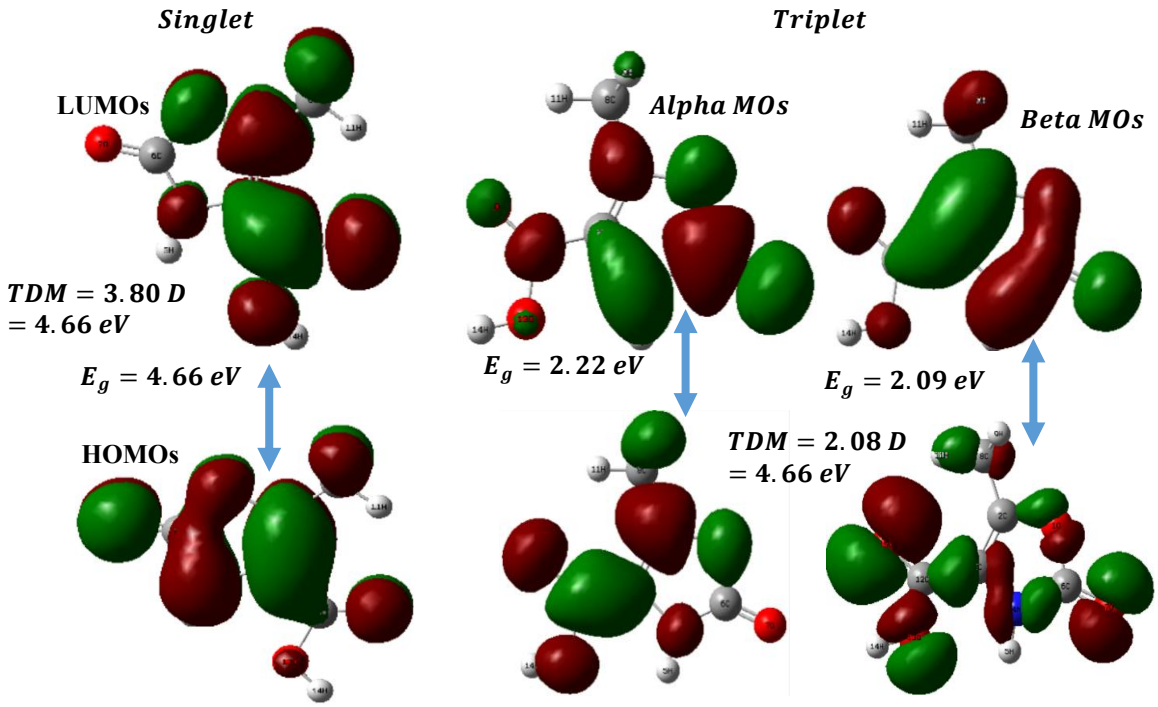


**Fig. 2.** FMOs in both singlet & triplet states for MOCA**.**

**Table 2.** MOCA Frontiers −Indices.

| **Parameter** | **B3LYP** | | |
|---|---|---|---|
| | **6~311G$^{(d,p)}$** | | |
| **Spin** | **Singlet** | **Triplet** | |
| | | **Alpha MOs** | **Beta MOs** |
| $E_{LUMO}$ $(eV)$ | -2.20 | -2.60 | -8.36 |
| $E_{HOMO}$ $(eV)$ | -6.85 | -4.81 | -10.45 |
| $E_{HOMO/LUMO}$ $(eV)$ | 4.66 | 2.22 | 2.09 |
| I = -$E_{HOMO}$ $(eV)$ | 2.20 | 2.60 | 8.36 |
| A = -$E_{LUMO}$ $(eV)$ | 6.85 | 4.81 | 10.45 |
| $\eta$= ½($E_{LUMO}$–$E_{HOMO}$) $(eV)$ | 2.33 | 1.11 | 1.05 |
| $\mu$= ½($E_{LUMO}$+ $E_{HOMO}$) $(eV)$ | -4.53 | -3.70 | -9.40 |
| $\psi = \mu^2/2\eta$ $(eV)$ | 4.40 | 6.19 | 42.29 |
| $\zeta = 1/\eta$ $(eV^{-1})$ | 0.43 | 0.90 | 0.96 |
| Electronegativity $\chi$ = -$\mu$ $(eV)$ | 4.53 | 3.70 | 9.40 |
| Total dipole~moment (D) | | | |

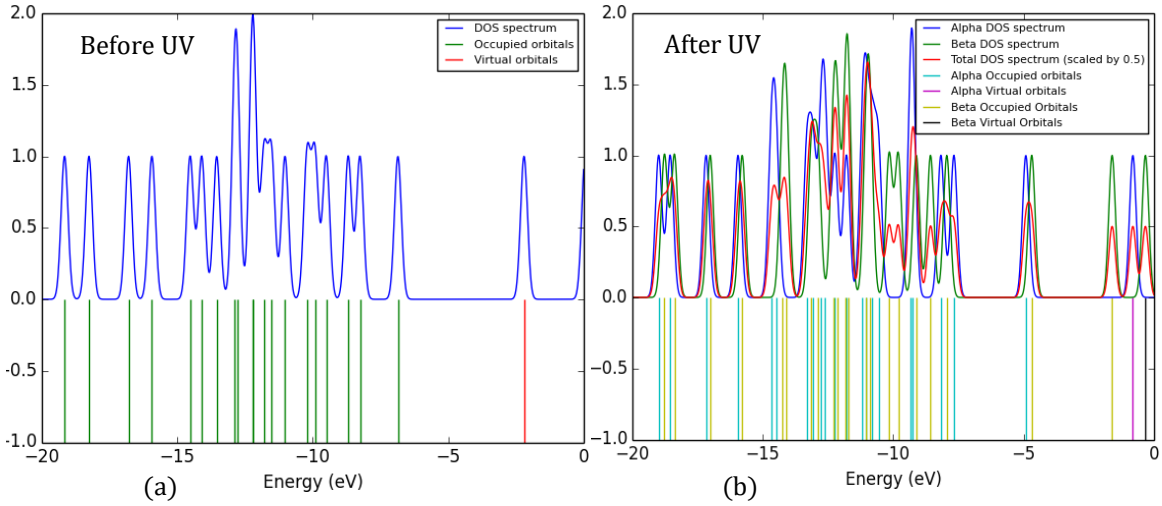


**Fig. 3**. Electronic DOS for (a) original and (b) illuminated MOCA.

This approach is commonly used in theoretical studies to investigate photoinduced effects when direct access to higher singlet states is computationally prohibitive. The choice of $T_1$ allows us to probe the system's response beyond the ground state while maintaining a reasonable computational cost.

These findings suggest that UV~irradiation not only alters the electronic properties of MOCA but also transforms its functional role from a wide-bandgap material to a potential candidate for use as a window layer in solar cells, where lower bandgaps are advantageous for efficient charge~transport and light transmission.

### 3.3. Polarizability and 1st~order hyperpolarizability anayses

To explore the correlation between molecular~architecture and nonlinear~optical (NLO) behavior, the static polarizability and 1$^{st}$~order hyperpolarizability of MOCA were computed through B3LYP/6-311G$^{(d,p)}$ level of theory within finite~field approximation.

The individual components of the polarizability tensor $\sum_{i,j} \alpha_{ii}$ and $\sum_{i,j,k} \beta_{ijk}$ were extracted from the Gaussian~output file generated during a frequency~calculation. From these tensor elements, key NLO descriptors—namely, mean~polarizability [$\alpha_{tot}$], polarizability~anisotropy [$\Delta\alpha$], and average first~order hyperpolarizability [$\beta_{tot}$] were derived via established equations [24-27]:

$$\alpha_{tot} = \frac{\alpha_{xx} + \alpha_{yy} + \alpha_{zz}}{3}$$

$$\Delta\alpha = \frac{1}{\sqrt{2}}\left[(\alpha_{xx} - \alpha_{yy})^2 + (\alpha_{yy} - \alpha_{zz})^2 + (\alpha_{zz} - \alpha_{xx})^2 + 6\alpha_{yz}^2 + 6\alpha_{xy}^2 + 6\alpha_{xz}^2\right]^{1/2}$$

$$\beta_{tot} = \left[(\beta_{xxx} + \beta_{xyy} + \beta_{xzz})^2 + (\beta_{yyy} + \beta_{yzz} + \beta_{yxx})^2 + (\beta_{zzz} + \beta_{zxx} + \beta_{zyy})^2\right]^{1/2}$$

The elevated values of dipole moment, molecular polarizability, and 1$^{st}$~order hyperpolarizability indicate strong nonlinear~optical (NLO) activity in MOCA. Such properties suggest that MOCA possesses significant potential for application in NLO devices, such as frequency~doublers, optical~switches, or electro~optic

modulators, where high response to external electric fields is essential. Table 3 presents the 1st~order hyperpolarizability [$\beta_{tot}$] along with [$\Delta\alpha$ & $\alpha_{tot}$] for original and irrdiated MOCA. The 1st ~order hyperpolarizability [$\beta_{tot(MOCA)}$] exhibits a significant decrease upon UV~exposure, reducing from $4.41 \times 10^{-30}$ esu to $3.66 \times 10^{-30}$ esu.

This reduction suggests that UV~irradiation may induce a partial loss of centrosymmetry or reduce the conjugation extent, thereby diminishing the hyperpolarizability. In comparison to urea, [$\beta_{tot(urea)} = 0.3728 \times 10^{-30}\ esu$], The $\beta_{tot(MOCA)}$ both before and after UV~exposure, is substantially higher than $\beta_{tot(urea)}$ [$\beta_{tot(MOCA)} \approx 11.8\ \beta_{tot(urea)}$ & $\beta_{tot(Irradiated\text{-}MOCA)} \approx 9.7\ \beta_{tot(urea)}$], respectively. This substantial enhancement indicates that MOCA is a promising candidate for NLO applications. Despite the decrease post-UV, The observed sensitivity to UV opens avenues for developing photoresponsive NLO materials, enabling dynamic control over optical properties in smart photonic devices.

**Table 3.** Mean~polarizability $\alpha_{tot}$ [$*10^{-24}\ esu$], anisotropy~polarizability $\Delta\alpha$ [$*10^{-24}\ esu$] & 1st~order hyperpolarizability $\beta_{tot}$ [$*10^{-30}\ esu$] for MOCA before and after UV-illumination.

| | **Before UV** | **After UV** | | **Before UV** | **After UV** |
|---|---|---|---|---|---|
| $\alpha_{xx}$ | 12.21 | 11.62 | $\beta_{xxx}$ | 0.39 | -0.94 |
| $\alpha_{xy}$ | -0.28 | 0.84 | $\beta_{xxy}$ | 0.57 | 0.84 |
| $\alpha_{yy}$ | 14.42 | 17.07 | $\beta_{xyy}$ | -1.75 | 0.33 |
| $\alpha_{xz}$ | -0.30 | -0.90 | $\beta_{yyy}$ | 3.62 | 2.70 |
| $\alpha_{yz}$ | -0.56 | -0.84 | $\beta_{xxz}$ | -0.04 | -0.08 |
| $\alpha_{zz}$ | 5.18 | 5.59 | $\beta_{xyz}$ | 0.09 | -0.24 |
| $\alpha_{tot}$ | 10.60 | 11.43 | $\beta_{yyz}$ | -0.14 | -0.34 |
| $\Delta\alpha$ | 8.44 | 10.27 | $\beta_{xzz}$ | 0.12 | 0.12 |
| | | | $\beta_{yzz}$ | 0.04 | 0.06 |
| | | | $\beta_{zzz}$ | -0.02 | -0.08 |
| | | | $\beta_{tot}$ | 4.41 | 3.66 |

## 4. Conclusion

This study presents a comprehensive computational investigation of 5-methyl-2-oxo-1,3-oxazolidine-4-carboxylic acid (MOCA) using Density Functional Theory (DFT) at the B3LYP/6-311G$^{(d,p)}$ level. The primary focus is on elucidating MOCA's structural, electronic, and nonlinear optical (NLO) properties, with particular attention to its behavior under UV illumination. Geometry optimization revealed key bond lengths and angles, establishing a stable molecular framework. Frontier Molecular Orbital (FMO) analysis demonstrated a significant reduction in the HOMO-LUMO energy gap upon UV exposure, from 4.66 eV in the ground state to approximately 2.09–2.22 eV in the excited triplet state. This narrowing indicates a transition from wide-bandgap characteristics to a more favorable configuration for charge transport, suggesting potential utility as a window layer in photovoltaic devices. The substantial narrowing of the HOMO-LUMO gap under UV exposure suggests enhanced intrinsic charge mobility, which may facilitate electron-hole recombination and improve charge transport efficiency. However, this prediction is based on computational estimates and should be validated experimentally through measurements of carrier mobility and conductivity.

Furthermore, the computed polarizability and first-order hyperpolarizability ($\beta_{tot}$) values indicate strong NLO activity; $\beta_{tot}$ decreased from $4.41 * 10^{-30}$ esu before UV to $3.66 * 10^{-30}$ esu after irradiation, yet remained substantially higher than that of urea ($0.3728 \times 10^{-30}$ esu), highlighting MOCA's promise for applications in frequency doubling, optical switching, or electro-optic modulation. The observed photoresponsiveness opens avenues for developing smart photonic materials with tunable optical properties. Overall, the findings underscore MOCA's multifunctional potential as an organic semiconductor with enhanced electronic and NLO characteristics, positioning it as a viable candidate for next-generation optoelectronic and photovoltaic technologies. This work fills a critical gap in the literature by providing the first theoretical exploration of MOCA's properties, offering a foundation for future experimental validation and material design.

## References


[1] D.R. Parmar, D.R. Merchant, S.V. Jadhav, Efficiency, materials, and cost-effectiveness of photovoltaic solar panels. *Powering Future: Clean Energy Solutions for a Sustainable Planet*, Springer (2025) 187–211. https://doi.org/10.1007/978-981-96-5055-2_12

[2] H. Bronstein, C.B. Nielsen, B.C. Schroeder, I. McCulloch, Context-dependent design of conjugated polymers. *Nat. Rev. Chem.*, 4 (2020) 66–77. https://doi.org/10.1038/s41570-019-0152-9

[3] L. Ma, S. Zhang, J. Wang, Y. Xu, J. Hou, High-efficiency organic solar cells. *Chem. Commun.*, 56 (2020) 14337–14352. https://doi.org/10.1039/D0CC05528J

[4] S.K. Garlapati, M. Divya, B. Breitung, R. Kruk, H. Hahn, S. Dasgupta, Electrolyte-gated transistors for organic electronics. *Adv. Mater.*, 30 (2018) 1707600. https://doi.org/10.1002/adma.201707600

[5] L. Nakka, Y. Cheng, A.G. Aberle, F. Lin, Recent progress in industrial silicon solar cells. *Adv. Energy Sustain. Res.*, 3 (2022) 2200045. https://doi.org/10.1002/aesr.202200045

[6] I. Joseph, H. Louis, T. Unimuke, I. Etim, M. Orosun, J. Odey, Review of solar energy systems and applications. *Appl. Sol. Energy*, 56 (2020) 334–363. https://doi.org/10.3103/S0003701X20050072

[7] A. Alhodaib, Z. Yahya, O. Khan, A. Equbal, M.S. Equbal, M. Parvez, et al., Computational study of the structural and electronic properties of materials. *Sci. Rep.*, 14 (2024) 11221. https://doi.org/10.1038/s41598-024-62048-5

[8] M. Tadesse, Y. Liu, Developments in catalytic systems for energy. *Catalysts*, 15 (2025) 571. https://doi.org/10.3390/catal15060571

[9] M. Ogbaje, V. Bhat, C. Risko, Computational materials research advances. *Annu. Rev. Mater. Res.*, 55 (2025). https://doi.org/10.1146/annurev-matsci-080423-011746
[10] T.A. Mukhtar, G.D. Wright, Mechanisms of antibiotic resistance. *Chem. Rev.*, 105 (2005) 529–542. https://doi.org/10.1021/cr030110z
[11] M. El-Mansy, M. Ismail, Spectroscopic and structural investigations of organic compounds. *Spectrochim. Acta A*, 135 (2015) 704–709. https://doi.org/10.1016/j.saa.2014.07.033
[12] M. El-Mansy, M. Ismail, Optical properties of thin films for solar applications. *Opt. Quantum Electron.*, 53 (2021) 103. https://doi.org/10.1007/s11082-021-02749-7
[13] M.J. Frisch, G.W. Trucks, H.B. Schlegel, G.E. Scuseria, M.A. Robb, J.R. Cheeseman, et al., Gaussian 09, Revision D.01. *Gaussian, Inc.*, Wallingford CT (2009).
[14] A. Frisch, R. Dennington, T. Keith, J. Millam, A. Nielsen, A. Holder, et al., GaussView, Release 5.0. *Gaussian, Inc.*, Wallingford CT (2009).
[15] R.G. Pearson, Absolute electronegativity and hardness: application to inorganic chemistry. *J. Chem. Educ.*, 65 (1988) 576–578.
[16] M. Koohi, H. Bastami, Adsorption of biologically active indoline-2-one on C20 nanocage. *Pramana*, 97 (2023) 143. https://doi.org/10.1007/s12043-023-02600-6
[17] M. Koohi, H. Bastami, Solvent effect on adsorption of benzylidene oxindole to C20 nanocage. *J. Phys. Org. Chem.*, 36 (2023) e4505. https://doi.org/10.1002/poc.4505
[18] M. Koohi, H. Bastami, Substituted Hammick carbenes: the effects of fused rings and hetero atoms. *J. Phys. Org. Chem.*, 33 (2020) e4023. https://doi.org/10.1002/poc.4023
[19] M. El-Mansy, M. Ibrahim, A. Suvitha, H. Abdelsalam, W. Osman, DFT and experimental study of some organic molecules. *Comput. Theor. Chem.*, 1202 (2021) 113343. https://doi.org/10.1016/j.comptc.2021.113343
[20] M. El-Mansy, A. Suvitha, B. Narayana, Computational study of electronic and optical properties. *Opt. Quantum Electron.*, 53 (2021) 424. https://doi.org/10.1007/s11082-021-03057-w
[21] M.A. El-Mansy, A.M. Bayoumy, H. Elhaes, M.A. Ibrahim, Structural and spectroscopic characterization of new compounds. *Opt. Quantum Electron.*, 55 (2023) 100. https://doi.org/10.1007/s11082-022-04353-9
[22] M. El-Mansy, O. Osman, A. Mahmoud, H. Elhaes, M. Ibrahim, Theoretical investigations of nano-structured materials. *Lett. Appl. NanoBioSci.*, 9 (2020) 1099–1102. https://doi.org/10.33263/LIANBS92.10991102
[23] M. Ibrahim, A. El-Barbary, M. El-Nahass, M. Kamel, M. El-Mansy, A. Asiri, Molecular structure and vibrational spectra of certain derivatives. *Spectrochim. Acta A*, 87 (2012) 202–208. https://doi.org/10.1016/j.saa.2011.11.039
[24] M.J. ElMansy, Advances in applied sciences and material characterization. *J. Umm Al-Qura Univ. Appl. Sci.*, 11 (2025) 746–756. https://doi.org/10.1007/s43994-024-00186-2
[25] M. El-Mansy, M. El-Nahass, Spectroscopic study of some solar cell materials. *Spectrochim. Acta A*, 130 (2014) 568–573. https://doi.org/10.1016/j.saa.2014.03.118
[26] M. El-Mansy, M. El-Bana, S. Fouad, Optical and structural properties of thin films. *Spectrochim. Acta A*, 176 (2017) 99–105. https://doi.org/10.1016/j.saa.2016.12.040
[27] M. El-Mansy, I. Yahia, Molecular structure and spectroscopic analysis of some complexes. *Spectrochim. Acta A*, 130 (2014) 59–63. https://doi.org/10.1016/j.saa.2014.03.113